Table 1 | Baseline clinical characteristics

No. of patients	51
Age (years)	68.5 ± 9.2
Male/Female	43/8
Alcohol intake (+/−)	18/33
Albumin (g/dL)	3.6 ± 0.5
Total bilirubin (mg/dL)	1.2 ± 0.7
Prothrombin time (INR)	1.2 ± 0.1
White cell count (/L)	4963 + 1894
Haemoglobin (g/dL)	12.6 ± 2.2
Platelet ($\times 10^9$/L)	150 ± 86
Chiid-Pugh class : A/B	26/25
HBV (+)/HCV (+)/HBV (−) and HCV (−)	6/39/6
Previous treatment (+/−)	35/16
Portal vein invasion (trunk/first branch/second branch)	11/18/22
Maximum tumour size (mm), (<100 mm/≥100 mm)	88.6 ± 32.1, 31/20
AFP (ng/mL) (≤1000/>1000, ≤10 000/>10 000)	29/10/12
AFP L3 (≧10%(%))	86.3%
DCP (mAU/mL) (≤1000/>1000, ≤10 000/>10 000)	14/20/17
Macroscopic finding (nodular/infiltrative)	15/36
Tumour location (unilobular/bilobular)	18/33

was performed to detect HCC. The right gastric artery and gastro-duodenal artery were embolized using microcoils (Diamond Coli, Boston Scientific; Trufill, Cordis; or Hilal Embolization Microcoils, Cook Europe) to prevent gastroduodenal injury by anti-cancer agents. A polyurethane-covered catheter (Anthron P-U Catheter, Toray Medical, Tokyo, Japan) was used as the indwelling catheter. The tip of the catheter was placed in the common hepatic artery or proper hepatic artery. The other end of the catheter was connected to the injection port and the device was implanted in a subcutaneous pocket. To prevent obstruction of the catheter, 5 mL (5000 U) of heparin solution was injected biweekly via the injection port.

Treatment protocol

The cisplatin-lipiodol plus 5-FU regimen comprised a combination of 50 mg cisplatin in 5–10 mL lipiodol and continuous infusion of 5-FU (1500 mg/5 days). At day 1 of treatment, cisplatin with lipiodol was injected through the reservoir catheter followed by 5-FU (250 mg). Then, 5-FU (1250 mg) was continuously infused using a balloon pump (SUREFUSER PUMP, Nipro Pharma Corporation, Osaka, Japan) for 5 days. This regimen was applied once a week during the first 2 weeks of admission, then the combination of 20 mg cisplatin with lipiodol and 5-FU (500–1250 mg) was infused every 2 weeks at the out-patient department (OPD) as long as possible. Chemotherapy was discontinued when adverse effects reached level 2 of the ECOG classification with the exception of platelet and leucocyte counts of<30 000/μL and 2000/μL respectively.

Assessment of response to chemotherapy

The primary efficacy endpoint was objective tumour response, while the secondary endpoint was patient survival. The primary efficacy endpoint was assessed at 3 months after the initial treatment and then every 2 months. At 3 months after initial treatment, partial responders and complete responders were distinguished. Tumours were bi-dimensionally measured by dynamic CT or dynamic MRI. The response to treatment was evaluated according to the Response Evaluation Criteria in Solid Tumours (RECIST)[22] and following the EASL[23] amendments that take into account the amount of necrotic tumour: as complete response (CR), all measureable lesions disappeared for more than 4 weeks; partial response (PR), sum longest diameter decrease more than 30% and no new lesion for more than 4 weeks; progressive disease (PD), sum longest diameter increase more than 25% or appearance of new lesion; stable disease (SD), no definition of PR and PD for more than 8 weeks.

Assessment of tolerability

Safety was assessed at each study visit, by adverse events, a brief physical examination, vital sign measurements and clinical laboratory evaluation. The severity of any toxicity was assessed according to the National Cancer Institute Common Toxicity Criteria, version 3. The presence of seven clinical symptoms and signs commonly noted in patients with HCC (ascites, anorexia, jaundice, local pain, lack of energy, malaise or bodily discomfort-fatigue and intratumoural haemorrhage) and complications associated with indwelling catheter (e.g. gastro-duodenal ulcer, infection, thrombosis and vascular damage) were also assessed.

Statistical analysis

Baseline data were expressed as mean ± s.d. or as median and range values. Survival was confirmed up to

© 2010 Blackwell Publishing Ltd

31 August 2009. Cumulative survival was calculated using the Kaplan–Meier method and compared by the log rank test. Independent factors for survival were assessed with the Cox proportional hazard regression model. Statistical significance was defined as a P value less than 0.05. The SPSS software version 14.0J (SPSS inc., Chicago, IL, USA) was used for statistical analysis.

RESULTS

Tumour characteristics

All patients were followed-up for more than 6 months. Tumour thrombosis was noted in the main portal vein in 10 patients, in the first branch in 18, and in the 2nd branch in 23 patients. The mean diameter of the main tumour was 87.0 mm (range, 50–170 mm). Serum α-fetoprotein (AFP) levels in 41 patients were >20 ng/mL. AFP-L3 was positive (>10%) in 32 patients, and 44 patients were des-γ-carboxy prothrombin (DCP)-positive (>40 AU/mL). Patients received 2–28 (median, 8.7) courses of cisplatin-lipiodol plus 5-FU therapy (Table 1).

Response to cisplatin-lipiodol plus 5-FU therapy and additional therapy

Of the 51 patients treated with this regimen, 10 (19.6%), 34 (66.7%) and 5 (9.8%) patients had a CR, PR and SD respectively [response rate (CR + PR/51) = 86.3%]. The remaining patient had PD. Of the 34 patients with PR, 24 were treated with surgical resection, RFA or TACE and showed the disappearance of visible HCC.

Survival and causes of death

Figure 1 shows the cumulative survival rates of 51 patients. The 12-, 24- and 36-month survival rates for the 51 patients were 72.9%, 58.1% and 34.9% respectively. The median survival rate of these patients was 33 (range, 3–51) months. The median survival time of CR, PR and SD patients were 39 (range, 13–51) months, 31 (range, 6–48) months and 7 (range, 4–23) months respectively. There was a significant difference in the survival time of the three groups. Figure 2 shows the cumulative survival rates of CR and PR patients, and SD and PD patients. The 12-, 24- and 36-month survival rates of the CR and PR patients were 78.4%, 61.8% and 37.1% respectively. There was a significant difference in the survival time between CR and PR patients and SD and PD patients. Figure 3 shows the cumulative survival rates of 10 patients with CR and 14 patients with PR who later showed disappearance of viable HCC after additional therapy and the remaining 27 patients who failed to be

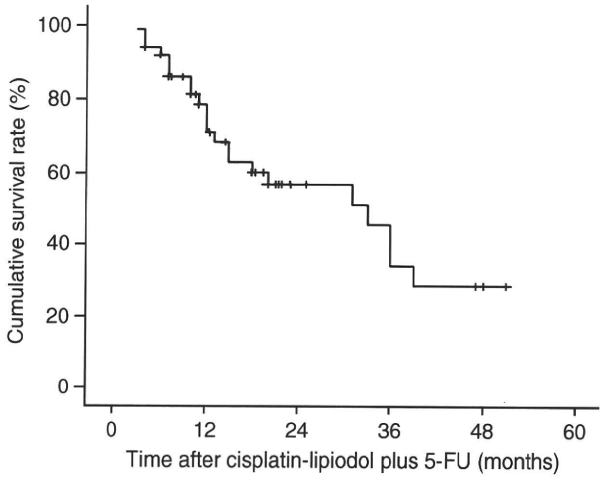

Figure 1 | Overall survival of all treated patients (n = 51).

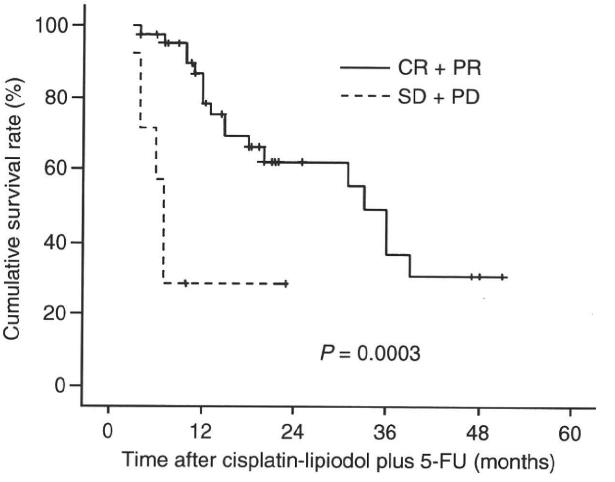

Figure 2 | Overall survival of patients who showed CR or PR and patients who showed SD or PD. CR, complete response; PR, partial response; SD, stable disease; PD, progressive disease. P = 0.0003 by Log Rank test.

tumour-free after additional therapy. The median survival time for the 24 patients who showed disappearance of viable HCC was 39 (range, 6–51) months. The 1-, 2- and 3-year survival rates of these patients were 100%, 89.5% and 53.7% respectively. On the other hand, the median survival time and 1-, 2- and 3-year survival rates of the remaining 27 patients were 12 (range, 3–25) months, and 44.8%, 24.0% and 0% respectively. There was a significant difference in survival between patients who showed disappearance of viable HCC and those with visible HCC during the treatment. Figure 4 displays the cumulative tumour progression-free survival time. The 6-, 12- and 24-month progression-free survival

© 2010 Blackwell Publishing Ltd

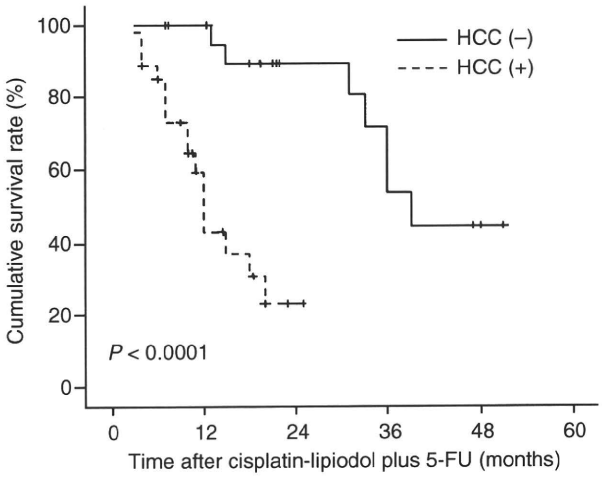

Figure 3 | Overall survival of patients who showed CR (n = 10) and disappearance of HCC after additional treatment (n = 14), and patients with variable HCC (n = 27). P = 0.0001 by Log Rank test; HCC (–), patients without variable HCC after treatment; HCC (+), patients with variable HCC after treatment; CR, complete response.

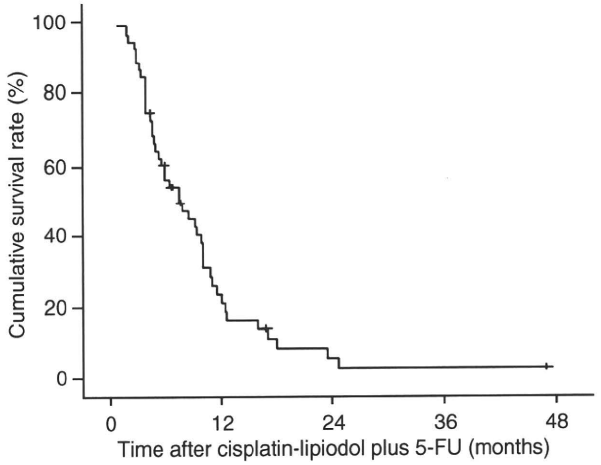

Figure 4 | Progression-free survival of all treated patients (n = 51).

rates of these patients were 62.1%, 21.9% and 11.7% respectively, with a median progression-free survival of 8.0 months. With regard to the relationship between survival and degree of tumour progression, there was no significant difference in median survival among patients with tumour thrombosis in the 2nd branches, the 1st branches and the portal vein trunk. With regard to the relationship between survival and liver damage, there was no significant difference in the median survival between patients with Child-Pugh class A and those with class B. During the follow-up period, 28 patients died. Of these, 24 died of tumour progression; two of rupture of oesophageal varices, one of liver failure and one patient died of renal failure.

Two of the 13 factors analysed by univariate analysis showed prognostic significance: tumour location (P = 0.048) and therapeutic effect (P < 0.001). Multivariate analysis identified only one variable, therapeutic effect, to be an independent predictor of mortality (P < 0.001) (Table 2).

Regarding the therapeutic effect, two of the 13 factors analysed by univariate analysis showed the therapeutic significance: tumour location (P = 0.042) and grade of portal vein invasion (P = 0.002). Multivariate analysis identified only one variable, grade of portal vein invasion, to be an independent predictor of therapeutic effect (P = 0.006) (Table 3).

Adverse effects and complications

No serious complications due to indwelling catheters, such as peptic ulcer, infection, thrombus and other vascular disorders, were observed. Treatment was not dis-

Table 2 | Univariate and multivariate analyses of survival for hepatocellular carcinoma

	HR (95% CI)	P value
Univariate analysis		
Gender (male)	1.24 (0.54-2.87)	0.609
Age (>65)	1.08 (0.32-3.65)	0.899
Alcohol intake (+)	1.15 (0.49-2.66)	0.752
HCV (positive)	0.50 (0.20-1.29)	0.152
HBV (positive)	2.03 (0.56-6.23)	0.218
Child-Pugh class (B)	1.12 (0.49-2.57)	0.786
AFP(ng/mL) (>1000)	1.51 (0.67-3.43)	0.322
DCP (AU/mL)(>1000)	1.03 (0.41-2.63)	0.946
Maximum tumour size (mm) (>100)	0.82 (0.34-2.01)	0.667
Macroscopic finding (infiltrative)	0.95 (0.39-2.31)	0.901
Tumour location (bilobular)	2.56 (1.01-6.48)	0.048
Grade of portal vein invasion (trunk)	1.62 (0.60-4.39)	0.344
Therapeutic effect (CR+PR)	0.17 (0.06-0.51)	0.001
Multivariate analysis		
Therapeutic effect (CR+PR)	0.21 (0.07-0.66)	0.007

© 2010 Blackwell Publishing Ltd

Table 3 | Univariate and multivariate analyses of therapeutic effect for hepatocellular carcinoma (CR+PR vs. SD+PD)

	Univariate analysis		
	CR+PR group (n = 44)	SD+PD group (n = 7)	P value
Gender (male/female)	38/6	6/1	0.963
Age (≤65/>65)	18/26	3/4	0.923
Alcohol intake (+/−)	16/28	2/5	0.689
HCV (+/−)	32/12	7/0	0.177
HBV (+/−)	6/38	0/7	0.578
Child-Pugh class (A/B)	23/21	3/4	0.703
AFP (ng/mL) (≤1000/1000-10 000/≥10 000)	26/9/9	3/1/3	0.431
DCP (AU/mL) (≤1000/1000-10 000/≥10 000)	14/16/14	0/4/3	0.211
Previous treatment (+/−)	14/30	1/6	0.658
Maximum tumour size (mm) (<100 mm/≥100 mm)	28/16	3/4	0.411
Macroscopic finding (nodular/infiltrative)	31/13	4/3	0.664
Tumour location (unilobular/bilobular)	18/26	0/7	0.042
Grade of portal vein invasion (trunk/first branch/second branch)	6/16/22	5/2/0	0.002

	Multivariate analysis		
	Hazard ratio	(95% CI)	P value
Grade of portal vein invasion	0.105	(0.02-0.52)	0.006

continued for serious complications. However, only one patient developed grade 3 thrombocytopaenia. Grade 1 appetite loss was noted in 17 patients, six patients developed grade 1 high fever and two developed grade 2 ascetic fluid accumulation. These adverse effects were controlled by medical treatment.

DISCUSSION

The prognosis of HCC patients with portal vein tumour thrombosis is very poor. Portal vein tumour thrombosis is a significant clinicopathological variable known to influence survival of patients with advanced HCC.[24] The median survival of untreated patients with HCC and portal vein tumour thrombosis is reported to be 2.7–4.0 months, whereas the survival of those without portal vein tumour thrombus is 24.4 months.[25, 26] To improve this bleak outcome, various treatments have been applied. Takizawa *et al.*[24] reported that the longest median survival (26.0 months) was associated with surgical resection, followed by continuous HAIC (8.0 months) and transcatheter arterial infusion/TAE (5.5 months). However, the number of patients with HCC and portal vein tumour thrombosis who are suitable for surgical resection is limited. In such situation, systemic chemotherapy, hormonal therapy and radiotherapy have all been reported to be of limited value.[27] Recently, two phase 3, double-blind, placebo-controlled trials designed to assess the efficacy of sorafenib for patients with advanced HCC were conducted.[12, 13] They demonstrated prolonged overall survival and time to progression in sorafenib-treated patients. Llovet *et al.*[21] propose the use of sorafenib as the 1st line treatment for patients with HCC categorized as BCLC C. However, in the SHARP trial, the median overall survival time of patients treated with sorafenib was 10.7 months.[12] In another study, the median overall survival of patients with portal vein tumour thrombosis was only 5 months.[15]

Trans-hepatic arterial infusion chemotherapy is a reasonable drug delivery system for patients with advanced HCC because advanced HCC receives most of its blood supply from the hepatic artery and non-cancerous liver is supplied mainly by the portal vein.[28] HAIC seems to deliver high concentrations of chemotherapeutic agents to HCC tissues selectively with low toxicity to non-cancerous liver tissues and whole body. Several reports described the effects of HAIC with cisplatin and 5-FU or systemic interferon-α therapy with HAIC using 5-FU for HCC patients with tumour thrombosis in the 1st branches and the portal

Aliment Pharmacol Ther 2010; 32: 543-550
© 2010 Blackwell Publishing Ltd

vein trunks. Although the response rate varied from 0% to 63%, the median survival time was less than 11.8 months.[16, 17, 19, 29–31] We also reported previously the efficacy of HAIC with cisplatin and 5-FU for HCC patients with portal vein tumour thrombosis. In that study, the response rate and median survival time were 48% and 10.2 months respectively.[17] Recently, Salem *et al.*[32] treated HCC patients with intra-arterial yttrium-90 microspheres. In their report, the median overall survival of patients with Child-Pugh class A and that of patients with class B who had portal vein tumour thrombosis were 10.4 and 5.6 months respectively. In the present study, the response rate was 86.3%. The degree of portal vein tumour thrombosis was a predictor of treatment effect. The overall survival rates at 12, 24 and 36 months were 72.9%, 58.1% and 34.9% respectively, and the overall median survival rate was 33 months. Univariate and multivariate analyses showed that only the therapeutic effect was an independent prognostic factor of survival. To the best of our knowledge, cisplatin-lipiodol plus 5-FU therapy is associated with the longest survival of HCC patients with portal vein tumour thrombosis in all studies reported so far. The rationale of cisplatin+5-FU regimen is that cisplatin and 5-FU have antitumour effects;[33] cisplatin has a synergistic effect as a modulator of 5-FU.[34] In HAIC with cisplatin and 5-FU or IFN and 5-FU, 5-FU is usually infused for 3–5 h.[17, 19, 30] In the present study, 5-FU was continuously infused for 5 days. 5-FU does not show a dose-dependent, but time-dependent antitumour effect.[35] Continuous infusion of 5-FU might enhance the antitumour effect in cisplatin-lipiodol plus 5-FU therapy compared with other HAICs. Anticancer agents in lipiodol suspension are reported to exhibit a more potent antitumour effect than anticancer agent alone.[36] Two possible mechanisms may explain this enhanced effect; embolization of tumour artery by lipiodol, and retention and continuous release in tumour tissues of anticancer agent. In the present study, a high concentration of cisplatin (9.8–13.5 μg/g wet tissue weight) was detected in the resected tumour tissues after 132 days of cisplatin with lipiodol injection. Furthermore, the concentration of cisplatin in tumour tissues was higher than that in adjacent non-tumour tissues (data not shown). The reason for the long median survival of patients participating in the present study could be the continuous infusion of 5-FU and use of cisplatin with lipiodol. In the present study, 24 patients showed disappearance of viable HCC (10 CR patients, 14 PR patients followed by additional therapy). The median survival time of these patients was significantly longer than that of patients with residual HCC. Cisplatin-lipiodol plus 5-FU therapy reduced tumour volume and allowed application of other treatments, thus prolonged survival even in HCC patients with PR. A recent study demonstrated that sorafenib prolongs the survival of patients with advanced HCC.[12] However, the response rate to sorafenib was extremely low.[12] Molecular targeted agents including sorafenib are probably not suitable to make tumour-free.

In the SHARP trial, approximately 52% of patients were reported to have grade 3 or grade 4 treatment-related toxicities, and the most common adverse events were diarrhoea (39%) and hand-foot skin reaction (21%).[12] As HCC is usually accompanied by liver cirrhosis, intensive chemotherapy sometimes induces severe liver damage, leucopaenia and thrombocytopaenia. However, in the present study, adverse events were less frequent than those reported recently in patients who received HAIC, TACE and sorafenib treatment.[12, 17, 37] Only one patient in our cohort developed grade 3 thrombocytopaenia. Furthermore, no deterioration of liver function or evidence of liver damage was noted. Although only two patients showed a transient increase in ascites, they were well controlled by medications. Thus, the adverse effects of this treatment were not serious and controllable.

In conclusion, the present study demonstrated the efficacy of HAIC using cisplatin in lipiodol and 5-FU, and that such therapeutic regimen for unresectable HCC with portal vein tumour thrombosis is not associated with serious adverse effects. The new HAIC can potentially become the first-line treatment for unresectable HCC with portal vein tumour thrombosis, subject to confirmation through a Phase III trial by comparison with sorafenib.

ACKNOWLEDGEMENT

Declaration of personal and funding interests: None.

REFERENCES

1. Cabrera R, Nelson DR. Review article: the management of hepatocellular carcinoma. *Aliment Pharmacol Ther* 2010; **31**: 461–76.
2. Parkin DM, Bray F, Ferlay J, *et al.* Global cancer statistics, 2002. *CA Cancer J Clin* 2005; **55**: 74–108.
3. Kiyosawa K, Umemura T, Ichijo T, *et al.* Hepatocellular carcinoma: recent trends in Japan. *Gastroenterology* 2004; **127**: S17–26.

© 2010 Blackwell Publishing Ltd

4. Llovet JM, Burroughs A, Bruix J. Hepatocellular carcinoma. *Lancet* 2003; **362**: 1907–17.
5. Llovet JM, Bruix J. Systemic review of randomized trial for unresectable hepatocellular carcinoma: chemoembolization improves survival. *Hepatology* 2003; **37**: 429–42.
6. Matsuda M, Suzuki T, Kono H, Fujii H. Predictors of hepatic venous trunk invasion and prognostic factors in patients with hepatocellular carcinomas that had come into contact with the trunk of major hepatic veins. *J Hepatobiliary Pancreat Surg* 2007; **14**: 289–96.
7. Stuart KE, Anand AJ, Jenkins RL. Hepatocellular carcinoma in the United States. Prognostic features, treatment outcome, and survival. *Cancer* 1996; **77**: 2217–22.
8. Portolani N, Coniglio A, Ghidoni S, *et al.* Early and late recurrence after liver resection for hepatocellular carcinoma: prognostic and therapeutic implications. *Ann Surg* 2006; **243**: 229–35.
9. Ikai I, Arii S, Kojiro M, *et al.* Reevaluation of prognostic factors for survival after liver resection in patients with hepatocellular carcinoma in a Japanese nationwide survey. *Cancer* 2004; **101**: 796–802.
10. Koike Y, Nakagawa K, Shiratori Y, *et al.* Factors affecting the prognosis of patients with hepatocellular carcinoma invading the portal vein – a retrospective analysis using 952 consecutive HCC patients. *Hepatogastroenterology* 2003; **50**: 2035–9.
11. Lopez P, Villanueva A, Llovet JM. Update systemic review of randomized controlled trials in hepatocellular carcinoma. 2002-2005. *Aliment Pharmacol Ther* 2006; **23**: 1535–47.
12. Llovet JM, Ricci S, Bruix J, *et al.* Sorafenib in advanced hepatocellular carcinoma. *N Engl J Med* 2008; **359**: 378–90.
13. Cheng AL, Kang YK, Chen Z, *et al.* Efficacy and safety of sorafenib in patients in the Asia-Pacific region with advanced hepatocellular carcinoma: a phase III randomised, double-blind, placebo-controlled trial. *Lancet Oncol* 2009; **10**: 25–34.
14. Wilhelm SM, Carter C, Tang L, *et al.* BAY 43-9006 exhibits broad spectrum oral anti-tumor activity and targets the Raf/MEK/ERK pathway and receptor tyrosine kinases involved in tumor progression and angiogenesis. *Cancer Res* 2004; **64**: 7099–109.
15. Yau P, Chan PNg KK, Chok SH, Cheung TT, Fan ST, Poon RT. Phase 2 open-label study of single agent sorafenib in treating advanced hepatocellular carcinoma in a hepatitis B-endemic Asian population. *Cancer* 2009; **115**: 428–36.
16. Itamoto T, Nakahara H, Tashiro H, *et al.* Hepatic arterial infusion of 5-fluorouracil and cisplatin for unresectable or recurrent hepatocellular carcinoma with tumor thrombus of the portal vein. *J Surg Oncol* 2002; **80**: 143–8.
17. Ando E, Tanaka M, Yamashita F, *et al.* Hepatic arterial infusion chemotherapy for advanced hepatocellular carcinoma with portal vein tumor thrombosis: analysis of 48 cases. *Cancer* 2002; **95**: 588–95.
18. Nagano H, Miyamoto A, Wada H, *et al.* Interferon-alpha and 5-fluorouracil combination therapy after palliative hepatic resection in patients with advanced hepatocellular carcinoma, portal venous tumor thrombus in the major trunk, and multiple nodules. *Cancer* 2007; **110**: 2493–501.
19. Obi S, Yoshida H, Toune R, *et al.* Combination therapy of intraarterial 5-fluorouracil and systemic interferon-alpha for advanced hepatocellular carcinoma with portal venous invasion. *Cancer* 2006; **106**: 1990–7.
20. Oken MM, Creech RH, Tormey DC, *et al.* Toxicity and response criteria of the Eastern Cooperative Oncology Group. *Am J Clin Oncol* 1982; **5**: 649–55.
21. Llovet JM, Di Bisceglie A, Bruix J, *et al.* Design and end-point of clinical trials in hepatocellular carcinoma. *J Natl Cancer Inst* 2008; **100**: 698–711.
22. Therasse P, Arbuck SG, Eisenhauer EA, *et al.* New guidelines to evaluate the response to treatment in solid tumors. European Organization for Research and Treatment of Cancer, National Cancer Institute of the United States, National Cancer Institute of Canada. *J Natl Cancer Inst* 2000; **92**: 205–16.
23. Bruix J, Sherman M, Llovet JM, *et al.* Clinical management of hepatocellular carcinoma. Conclusions of the Barcelona-2000 EASL conference. European Association for the Study of the Liver. *J Hepatol* 2001; **35**: 421–30.
24. Takizawa D, Kakizaki S, Sohara N, *et al.* Hepatocellular carcinoma with portal vein tumor thrombosis: clinical characteristics, prognosis, and patient survival analysis. *Dig Dis Sci* 2007; **52**: 3290–5.
25. Llovet JM, Bustamante J, Castells A, *et al.* Natural history of untreated nonsurgical hepatocellular carcinoma: rationale for the design and evaluation of therapeutic trials. *Hepatology* 1999; **29**: 62–7.
26. Pawarode A, Voravud N, Sriuranpong V, *et al.* Natural history of untreated primary hepatocellular carcinoma: a retrospective study of 157 patients. *Am J Clin Oncol* 1998; **21**: 386–91.
27. Llovet JM. Updated treatment approach to hepatocellular carcinoma. *J Gastroenterol* 2005; **40**: 225–35.
28. Breedis C, Young G. The blood supply of neoplasms in the liver. *Am J Pathol* 1954; **30**: 969–77.
29. Yamasaki T, Kurokawa F, Shirahashi H, *et al.* Novel arterial infusion chemotherapy using cisplatin, 5-fluorouracil, and leucovorin for patients with advanced hepatocellular carcinoma. *Hepatol Res* 2002; **23**: 7–17.
30. Sakon M, Nagano H, Dono K, *et al.* Combined intraarterial 5-fluorouracil and subcutaneous interferon-alpha therapy for advanced hepatocellular carcinoma with tumor thrombi in the major portal branches. *Cancer* 2002; **94**: 435–42.
31. Ota H, Nagano H, Sakon M, *et al.* Treatment of hepatocellular carcinoma with major portal vein thrombosis by combined therapy with subcutaneous interferon-alpha and intra-arterial 5-fluorouracil; role of type 1 interferon receptor expression. *Br J Cancer* 2005; **93**: 557–64.
32. Salem R, Lewandowski RJ, Mulcahy MF, *et al.* Radioembolozation for hepatocellular carcinoma using yttrium-90 microspheres: a comprehensive report of long-term outcomes. *Gastroenterology* 2010; **138**: 52–64.
33. Paquet KJ, Kalk JF, Cuan-Orozco F, *et al.* Hepatic chemoinfusion of 5-FU in metastasis of gastrointestinal cancer and advanced primary hepatocellular carcinoma. *Eur J Surg Oncol* 1992; **18**: 156–61.
34. Hata F, Sasaki K, Hirata K, Yamamitsu S, Shirasaka T. Efficacy of a continuous venus infusion of fluorouracil and daily dividedc dose cisplatin as adjuvant therapy in resectable colorectal cancer: a prospective randomized trial. *Surg Today* 2008; **38**: 623–32.
35. Okabe H, Toko T, Saito H, *et al.* Augmentation of the chemotherapeutic effectiveness of UFT, a combination of tegafur [1-(2-tetrahydrofuryl)-5-fluorouracil] with uracil, by oral l-leucovorin. *Anticancer Res* 1997; **17**: 157–64.
36. Terayama N, Matsui O, Gabata T, *et al.* Accumulation of iodized oil within the nonneoplastic liver adjacent to hepatocellular carcinoma via the drainage routes of the tumor after transcatheter arterial embolization. *Cardiovasc Intervent Radiol* 2001; **24**: 383–7.
37. Buijs M, Vossen JA, Frangakis C, *et al.* Nonresectable hepatocellular carcinoma: long-term toxicity in patients treated with transarterial chemoembolization-single-center experience. *Radiology* 2008; **249**: 346–54.

Aliment Pharmacol Ther 2010; 32: 543-550
© 2010 Blackwell Publishing Ltd

Cardiovasc Intervent Radiol
DOI 10.1007/s00270-010-0036-3

CLINICAL INVESTIGATION

Angiographic Evaluation of Feeding Arteries of Hepatocellular Carcinoma in the Caudate Lobe of the Liver

Shiro Miyayama · Masashi Yamashiro · Yuki Hattori · Nobuaki Orito · Ken Matsui · Kazunobu Tsuji · Miki Yoshida · Osamu Matsui

Received: 12 July 2010 / Accepted: 24 October 2010
© Springer Science+Business Media, LLC and the Cardiovascular and Interventional Radiological Society of Europe (CIRSE) 2010

Abstract
Purpose To evaluate the origins of feeders of hepatocellular carcinoma (HCC) in the caudate lobe (S1).
Materials and Methods Eighty-eight HCCs (mean diameter 21.4 mm) were treated by chemoembolization. The tumor-feeding caudate artery was confirmed when a tumor stain was demonstrated on angiogram and iodized oil was accumulated into the HCC and S1 on computed tomography (CT). The origins were divided into R_1 (right proximal), R_2 (right distal), L_1 (left proximal), L_2 (left distal), A (anterior segmental), P (posterior segmental), M (middle hepatic or medial segmental), Ph (proper hepatic), Ch (common hepatic), and Ex (extrahepatic). The origins of feeders supplying HCCs in the Spiegel lobe (SP; $n = 36$), the paracaval portion (PC; $n = 38$), and the caudate process (CP; $n = 14$) were also analyzed.
Results One hundred sixteen feeders were identified: 11 (9.5%) arose from R_1; 21 (18.1%) arose from R_2; nine arose (0.9%) from L_1; 15 (12.9%) arose from L_2; 24 (20.7%) arose from A; 25 (21.6%) arose from P; seven (6.0%) arose from M; one (0.9%) arose from Ph; and three (2.6%) arose from Ex. HCCs in the SP and the PC were fed by feeders from both hepatic arteries (the ratios of right to left were 3:2 and 3:1, respectively), and HCCs in the CP were dominantly fed by feeders from the right hepatic artery.
Conclusion The caudate artery most frequently arises from the right hepatic artery, followed with almost equal frequency by the left hepatic, the anterior segmental, and the posterior segmental artery. The origins of the caudate arteries differ according to the subsegmental locations.

Keywords Hepatocellular carcinoma · Caudate lobe · Feeding artery · Transcatheter arterial chemoembolization

Introduction

The caudate lobe is centrally located in the liver between the right and left lobes of the liver and near the hepatic hilus and the inferior vena cava. Because of this anatomic location, hepatocellular carcinoma (HCC) arising in the caudate lobe is difficult to treat [1]. Surgical resection of the caudate lobe has a high mortality rate because of large amounts blood loss, a high rate of postoperative complications, and a high tumor-recurrence rate [2, 3]. Percutaneous ablation therapy, such as ethanol injection and radiofrequency ablation, is a useful alternative treatment [4–6]; however, the procedure might be technically difficult because of the deep tumor location and adjacent large vessels. Therefore, transcatheter arterial chemoembolization (TACE) plays an important role in the treatment of HCC in the caudate lobe, although local tumor recurrence is frequently observed after TACE [4, 7, 8].

Because there are usually multiple caudate arteries arising from the right, left, and middle hepatic arteries, as well as from the extrahepatic collateral vessels, 16–31% of HCCs in the caudate lobe are fed by multiple branches arising from different origins [7–12]. These factors might make it more difficult to control HCC in the caudate lobe using TACE [7, 8, 10]. Recognition of vascular anatomy

S. Miyayama (✉) · M. Yamashiro · Y. Hattori · N. Orito · K. Matsui · K. Tsuji · M. Yoshida
Department of Diagnostic Radiology, Fukuiken Saiseikai Hospital, Fukui, Japan
e-mail: s-miyayama@fukui.saiseikai.or.jp

O. Matsui
Department of Radiology, Kanazawa University Graduate School of Medical Science, Kanazawa, Japan

Published online: 18 November 2010

supplying HCCs in the caudate lobe is key to performing effective TACE. Thus, the purpose of our study was to retrospectively analyze the origins of the HCC-feeding arteries in the caudate lobe and to evaluate the anatomic variations of tumor-feeding arteries in relation to subsegments of the caudate lobe.

Materials and Methods

We performed a retrospective study to evaluate the origins of tumor-feeding caudate arteries. This was a retrospective study using imaging data and clinical records with no change in patient care; Institutional Review Board approval is not required at our institution for this type of study. Written informed consent was obtained from each patient before the TACE procedure.

Patients

Between February 2002 and February 2010, 88 HCCs originating in the caudate lobe were detected in 84 patients. There were 48 men and 36 women, and the mean patient age was (mean ± SD) 70.2 ± 7.3 years (range 45–86). All patients had liver cirrhosis. This was related to hepatitis C in 71 patients, to hepatitis B in four patients, and to alcohol in three patients. The etiology was unknown in six patients. The diagnosis of HCC was established by imaging findings: (1) characteristic nodular enhancement on the arterial phase and wash out on the delayed phase images on computed tomography (CT) and/or magnetic resonance imaging; (2) nodular stain on angiography and/or CT during hepatic arteriography obtained using conventional CT or cone-beam CT; and (3) nodular perfusion defect on CT during arterial portography obtained using conventional CT or cone-beam CT. Histological confirmation was not obtained in any patient in this series. Mean tumor diameter was 21.4 ± 11.0 mm (range 8–62). Fifty-two patients (61.9%) had a history of TACE for HCC before detection of HCC in the caudate lobe. Thirty-two patients (38.1%) had no treatment history for HCC.

Hepatic Angiography and the TACE Procedure

Arteriograms of the celiac and superior mesenteric arteries were routinely performed using a 4F catheter. Common hepatic or proper hepatic arteriogram was also performed in all patients using a 4F catheter or a 1.8F-tip (Carnelian Pixie; Tokai Medical Products, Kasugai, Japan), a 2F-tip (Progreat α; Terumo, Tokyo, Japan), or a 2.4F-tip (Microferret; Cook, Bloomington, IN, USA) microcatheter. Arteriograms of extrahepatic vessels, such as the right inferior phrenic artery, the right renal capsular artery, and the left gastric artery, were obtained when the tumor stain was unclear on hepatic arteriography.

All TACE procedures performed through the caudate arteries were selectively performed using a microcatheter. The microcatheter with its tip bent into a J shape by steam was used for all procedures to facilitate insertion into small caudate arteries that branched at acute angles. To navigate the microcatheter, a 0.016-inch guidewire (GT-wire; Terumo) was used. When selection of the feeding branch by the 0.016-inch guidewire was difficult, a 0.012-inch guidewire (GT-wire; Terumo) was used. After the microcatheter was inserted into the target branch, 0.5 ml 2% lidocaine (Xylocaine; Fujisawa, Osaka, Japan) was intra-arterially injected to prevent pain and vasospasm. First, a mixture of 2–4 ml iodized oil (Lipiodol; Andre Guerbet, Aulnaysous-Bois, France) and anticancer drugs (10–20 mg epirubicin [Farmorbicin; Kyowa Hakko, Tokyo, Japan] and 2–4 mg mitomycin C [Mitomycin; Kyowa Hakko]) was injected and this was followed by injection of gelatin sponge particles. The total amount of iodized oil injected in a single procedure was determined based on the tumor size (volume almost equal to the diameter of the tumor, e.g., a 3-cm tumor received 3 ml iodized oil). Until December 2006, gelatin sponge (Gelfoam; Upjohn, Kalamazoo, MI, USA) particles that were cut into approximately 1-mm cubes were used. Since January 2007, commercially available gelatin sponge particles (Gelpart; Nippon Kayaku, Tokyo, Japan) 1 mm in diameter have been used. TACE through extrahepatic collateral vessels was also performed when the blood supply to the tumor was demonstrated. Unenhanced CT was obtained 1 week after TACE in all patients to check for iodized oil accumulation in HCCs in the caudate lobe.

Definition of the Origin of the Caudate Artery

We defined the embolized branch as the tumor-feeding caudate artery when a tumor stain was demonstrated on arteriogram and iodized oil showed accumulation in the HCC and the caudate lobe on CT obtained 1 week after TACE. If CT 1 week after TACE showed a tumor portion in which iodized oil was not accumulated, an additional TACE was performed 2–6 months later according to the residual tumor size and patient's medical condition. When the residual tumor was supplied by another caudate artery that had initially not been embolized, the caudate artery was also defined as the tumor-feeding caudate artery.

The origins of the caudate arteries were divided into R_1, R_2, L_1, L_2, A, P, M, Ph, Ch, and Ex (Fig. 1). The caudate lobe was divided into three subsegments according to the classification proposed by Kumon [13] (Fig. 2): the Spiegel lobe (SP), the paracaval portion (PC), and the caudate process (CP). The origins of the caudate arteries supplying

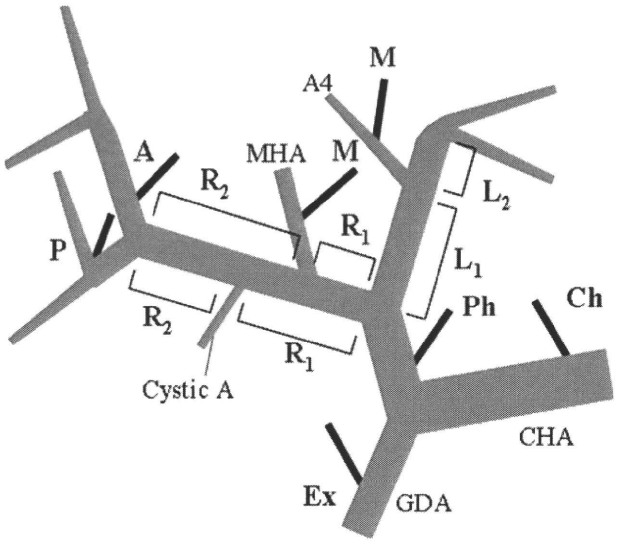

Fig. 1 The definition of the origins of tumor-feeding caudate arteries. R_1 (*right proximal*) arising from the right hepatic artery (RHA) between its origin and the middle hepatic artery (MHA) bifurcation or the cystic artery bifurcation if the MHA was not present; R_2 (*right distal*) arising from the RHA between the MHA (or cystic artery) bifurcation and the bifurcation of the anterior and posterior segmental artery of the RHA. If both the MHA and the cystic artery were not present, the RHA was divided into the two equal parts; L_1 (*left proximal*) arising from the left hepatic artery (LHA) between its origin and the medial segmental artery (A4) bifurcation; L_2 (*left distal*) arising from the LHA between the A4 bifurcation and the umbilical portion of the LHA. If the A4 did not arise from the LHA, the LHA was divided into the two equal parts; *A* arising from the anterior segmental artery of the right hepatic artery; *P* arising from the posterior segmental artery of the right hepatic artery; *M* arising from the MHA or the A4; *Ph* arising from the proper hepatic artery; *Ch* arising from the common hepatic artery; and *Ex* arising from the extrahepatic vessels

the HCCs in each subsegment were also analyzed. When a tumor was located between two subsegments, the tumor was classified based on the one subsegment in which it was dominantly located.

Results

Origins of the Tumor-Feeding Caudate Arteries

Eighty-two tumors in the caudate lobe of 78 patients were treated by a single TACE session. The remaining six tumors in six patients were treated with two TACE sessions because of incomplete iodized oil accumulation in the entire tumor on CT obtained after the initial TACE session. In total, 116 caudate arteries were identified, and all were selectively embolized during TACE, including six additional TACE sessions (Table 1). During TACE, 1.3 ± 0.5 feeding arteries (range 1–3) were embolized/tumor. Eleven caudate arteries (9.5%) were derived from R_1; 21 (18.1%) from R_2; nine (7.8%) from L_1; 15 (12.9%) from L_2; 24 (20.7%) from A; 25 (21.6%) from P; seven (6.0%) from M; one (0.9%) from Ph; and three (2.6%) from Ex. No caudate arteries were derived from Ch in the present series. Eighty-one caudate arteries (70.4%) were derived from the right hepatic arterial system ($R_1 + R_2 + A + P$), and 31 (27.0%) were derived from the left hepatic arterial system ($L_1 + L_2 + M$). In total, 27.6% of the caudate arteries were derived from the right hepatic artery ($R_1 + R_2$), 20.7% from the left hepatic artery ($L_1 + L_2$), 20.7% from the anterior segmental artery of the right hepatic artery, 21.6% from the posterior segmental artery of the right hepatic artery, and 6.0% from the middle hepatic artery or the medial segmental artery.

Origins of the Caudate Arteries Supplying HCCs in the SP

Our findings are listed in Table 2. There were 36 tumors with a mean diameter of 22.3 ± 11.9 mm (range 8–62 mm) in the SP. Twenty-five tumors (69.4%) were supplied by a single tumor-feeding caudate artery. Among these, 15 tumors were supplied by the feeding artery derived from the right hepatic arterial system (R_1 [$n = 2$], R_2 [$n = 7$], A [$n = 2$], P [$n = 4$]) (Fig. 3), and nine were supplied by the feeding artery derived from the left hepatic arterial system (L_1 [$n = 3$], L_2 [$n = 4$], M [$n = 2$]). The remaining tumor was supplied by a feeding artery derived from the right inferior phrenic artery (Ex). Eleven tumors (30.6%) had two feeding arteries. Among these, eight were supplied by feeding arteries derived from the right (R_1 [$n = 2$], R_2 [$n = 1$], A [$n = 4$], P [$n = 1$]) and the left hepatic arterial system (L_1 [$n = 3$], L_2 [$n = 4$], M [$n = 1$]), respectively (Figs. 4 and 5). One tumor was supplied by two feeding arteries derived from A. The remaining two tumors were supplied by feeding arteries derived from the left hepatic arterial system (L_2 [$n = 1$], M [$n = 1$]) and Ex (the right inferior phrenic artery [$n = 1$] as well as the accessory left gastric artery [$n = 1$]), respectively. In total, there were 47 tumor-feeding caudate arteries. Twenty-five tumor-feeding arteries arose from the right hepatic arterial system, 19 from the left hepatic arterial system, and three from the extrahepatic collaterals. The diameters of three tumors that were supplied by extrahepatic collaterals were 17, 26, and 48 mm, respectively. All three tumors were detected in patients with no histories of TACE, including one patient who had undergone hepatic resection. All three tumors were located at the anterior ($n = 1$) or posterior ($n = 2$) surface of the SP.

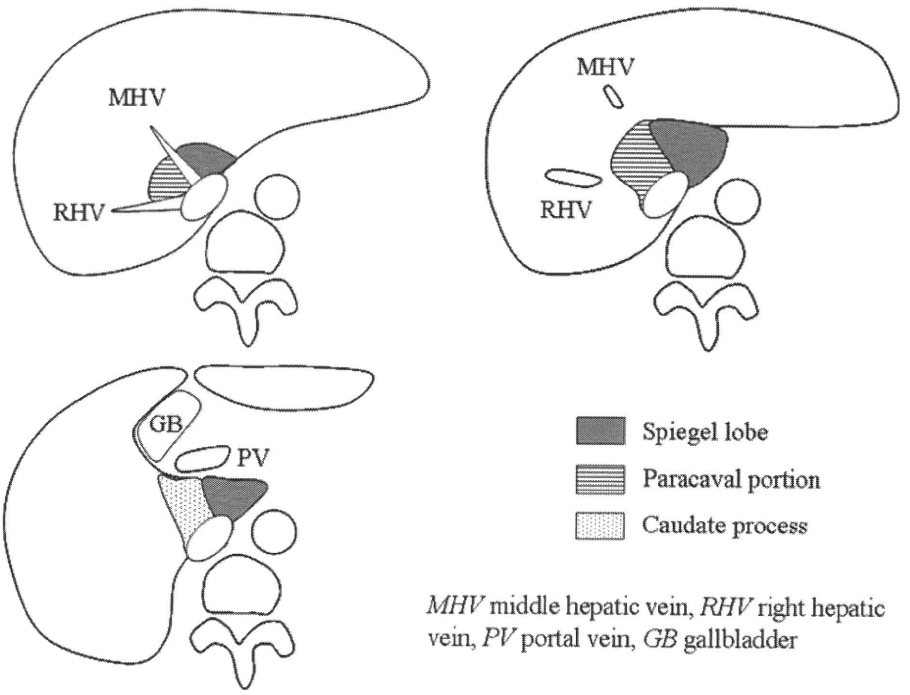

Fig. 2 Schematic presentation of subsegments of the caudate lobe

Table 1 Origins of tumor-feeding arteries of 88 HCCs in the caudate lobe

Origin	No. (%)	
R_1	11 (9.5)	32 (27.6%)
R_2	21 (18.1)	
L_1	9 (7.8)	24 (20.7%)
L_2	15 (12.9)	
A	24 (20.7)	
P	25 (21.6)	
M	7 (6.0)	
Ph	1 (0.9)	
Ch	0 (0)	
Ex	3 (2.6)	
Total	116 (1.3 ± 0.5 arteries/tumor)	

Mean tumor diameter 21.4 ± 11.0 mm [range 8–62]

Origins of the Caudate Arteries Supplying HCCs in the PC

Our findings are listed in Table 3. There were 38 tumors with a mean diameter of 20.2 ± 9.3 mm (range 8–47) in the PC. Twenty-nine tumors (76.3%) were supplied by a single feeding artery. Among these, 20 tumors were supplied by the caudate artery derived from the right hepatic arterial system (R_1 [$n = 4$], R_2 [$n = 7$], A [$n = 3$], P [$n = 6$]). Nine were supplied by the caudate artery derived from the left hepatic arterial system (L_1 [$n = 1$], L_2 [$n = 5$], M [$n = 3$]). Seven tumors (18.4%) had two feeding arteries. Among these, three tumors were supplied by feeding arteries derived from the right (A [$n = 1$], P [$n = 2$]) and the left hepatic arterial system (L_1 [$n = 2$], L_2 [$n = 1$]), respectively. Four tumors were supplied by two feeding arteries derived from the right hepatic arterial system (R_2 and P [$n = 1$], A × 2 [$n = 1$], A and P

Table 2 Feeding arteries of 36 HCCs in the SP

No. of feeders	No. of tumors (%)	Site	Origin	Tumor
1	25 (69.4)	R	R_1	2
			R_2	7
			A	2
			P	4
		L	L_1	3
			L_2	4
			M	2
		Ex	Ex[a]	1
2	11 (30.6)	R + L	R_1, L_1	1
			R_1, L_2	1
			R_2, L_1	1
			A, L_1	1
			A, L_2	2
			A, M	1
			P, L_2	1
		R × 2	A × 2	1
		L + Ex	L_2, Ex[b]	1
			M, Ex[a]	1

Mean tumor diameter 22.3 ± 11.9 mm [range 8–62]. The ratio of R:L = 25:19

[a] Arising from the right inferior phrenic artery

[b] Arising from the accessory left gastric artery

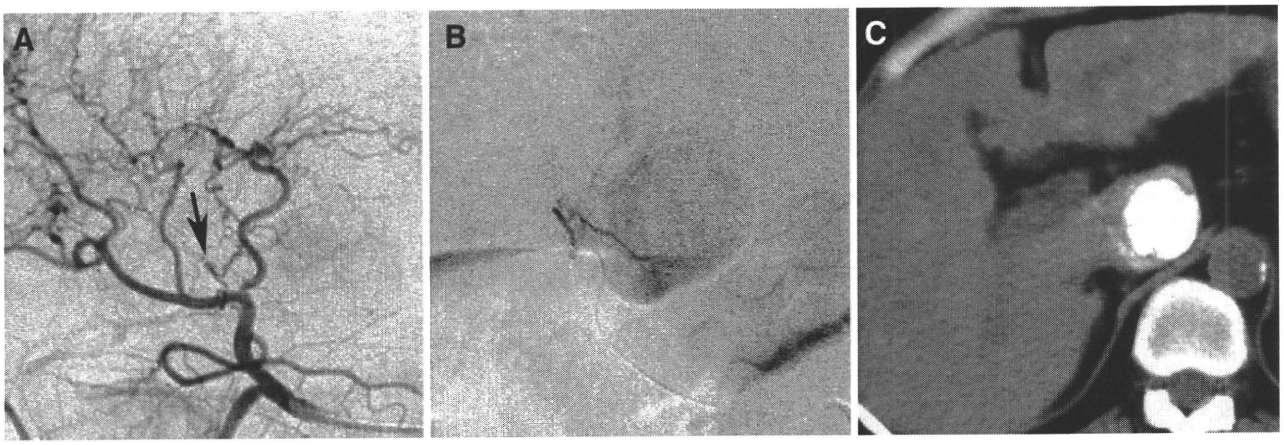

Fig. 3 A 45-year-old woman with HCC in the SP. **A** Common hepatic arteriogram showed that the caudate artery derived from the right hepatic artery proximal to the middle hepatic artery (*arrow*). **B** The caudate artery was selected, and TACE was performed. **C** CT obtained 1 week after TACE showed dense iodized oil accumulation in HCC in the SP

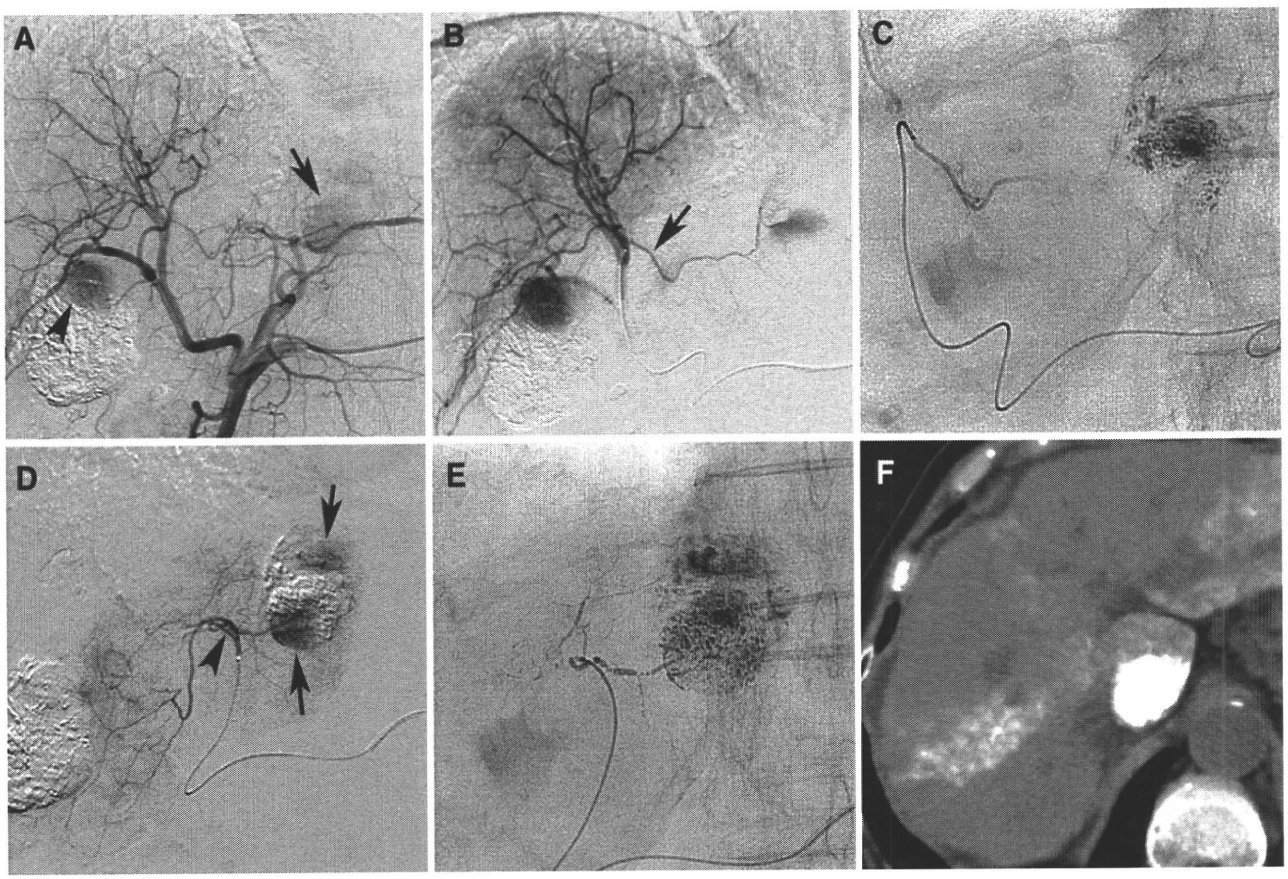

Fig. 4 A 73-year-old woman with HCC in the SP. **A** Common hepatic arteriogram showed tumor stains in the caudate lobe (*arrow*) and in the right lobe near the previously embolized tumor (*arrowhead*). **B** Arteriogram of the anterior segmental artery of the right hepatic artery showed tumor stains. The arrow shows the caudate artery. **C** The caudate artery was selected, and TACE was performed. Subsequently, the tumor in the right lobe was also embolized (not shown). **D** Arteriogram of the medial segmental artery showed a residual tumor stain of HCC in the caudate lobe (*arrows*). The *arrowhead* shows the caudate artery. **E** The caudate artery was selected, and TACE was performed. **F** CT obtained 1 week after TACE showed dense iodized oil accumulation in HCC in the SP

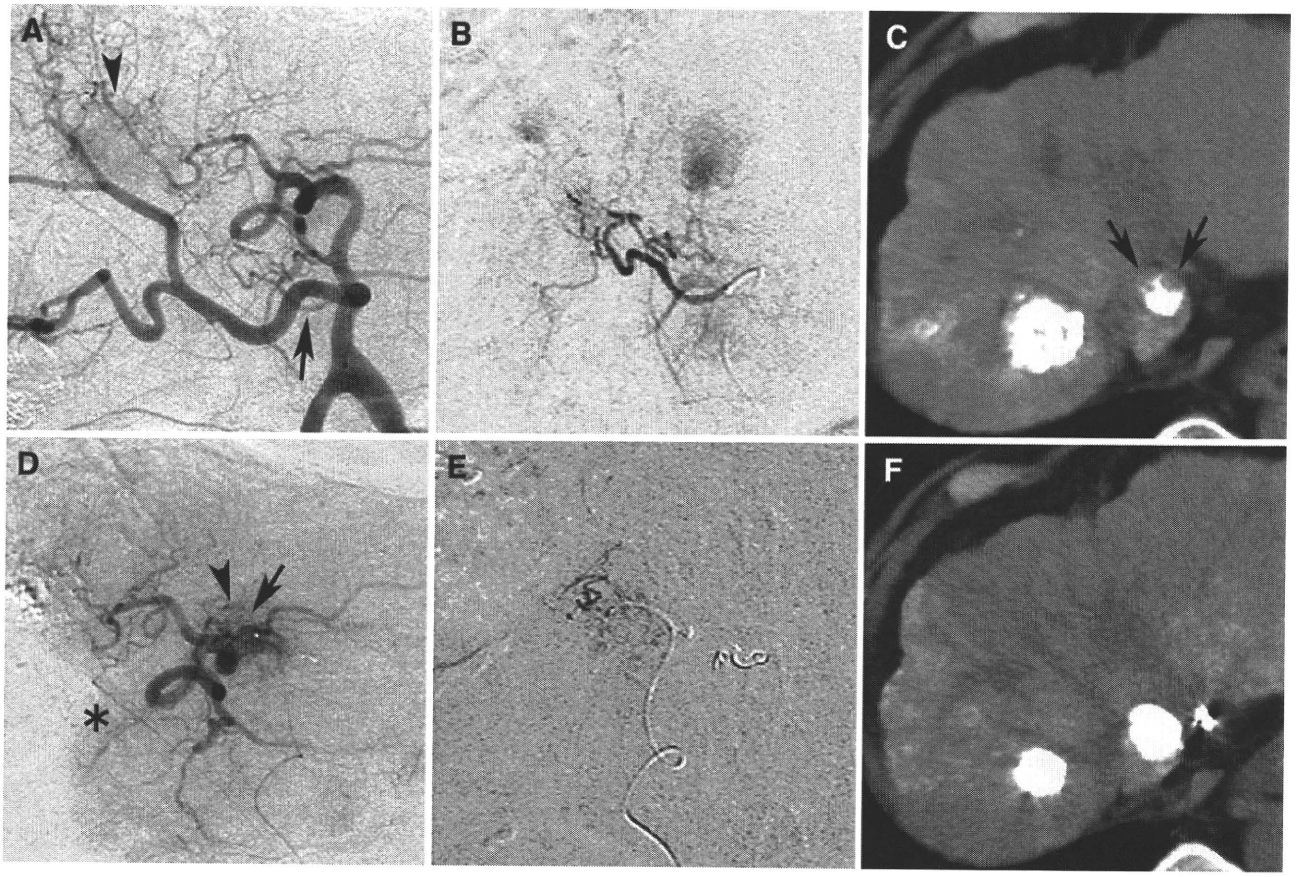

Fig. 5 A 78-year-old man with HCC in the SP. **A** Common hepatic arteriogram showed that the caudate artery derived from the proximal right hepatic artery (*arrow*). Another tumor stain in the right lobe of the liver was also seen (*arrowhead*). **B** Selective arteriogram of the caudate artery showed two tumor stains. This vessel was embolized. Subsequently, the tumor in the right lobe was also embolized (not shown). **C** CT obtained 1 week after TACE showed that iodized oil was densely accumulated in the tumor in the SP, but a tumor portion without iodized oil accumulation was seen (*arrows*). Iodized oil was also densely accumulated other tumors in the right lobe of the liver. **D** Arteriogram of the left hepatic artery obtained 4 months after initial TACE showed that the caudate artery derived from the distal left hepatic artery (*arrow*), and a residual tumor stain (*arrowhead*) was seen. The falciform artery was also seen (*asterisk*). **E** The caudate artery was selected and embolized. **F** CT obtained 1 week after second TACE showed dense iodized oil accumulation in the entire tumor

[$n = 2$]). The remaining two tumors (5.3%), which were 14 and 23 mm in diameter, respectively, were supplied by three feeding arteries derived from the right hepatic arterial system at R_1, A, and P and R_2, A, and P, respectively (Fig. 6). In total, there were 49 tumor-feeding caudate arteries. Thirty-seven tumor-feeding caudate arteries arose from the right hepatic arterial system, and 12 arose from the left hepatic arterial system.

Origins of the Caudate Arteries Supplying HCCs in the CP

Our findings are listed in Table 4. There were 14 tumors with a mean diameter of 21.8 ± 12.9 mm (range 12–49) in the CP. Nine tumors (64.3%) were supplied by a single feeding artery. Among these, seven tumors were supplied by a feeding artery derived from the right hepatic arterial system (R_1 [$n = 1$], A [$n = 3$], P [$n = 3$]) (Fig. 7); one was supplied by the caudate artery derived from M; and one was supplied by the caudate artery derived from Ph. Four tumors were supplied by two feeding arteries derived from the right hepatic arterial system (R_1 and R_2 [$n = 1$], R_2 and A [$n = 1$], A × 2 [$n = 1$], P × 2 [$n = 1$]). The remaining tumor (7.1%), which was 13 mm in diameter, was supplied by three feeding arteries derived from the right hepatic arterial system at R_2, P, and P, respectively. In total, there were 20 tumor-feeding caudate arteries. Eighteen tumor-feeding arteries arose from the right hepatic arterial system; one arose from the middle hepatic artery; and one arose from the proper hepatic artery.

Discussion

A cadaver dissection study by Mizumoto et al. [10] reported that the caudate arteries arose from the posterior

Table 3 Feeding arteries of 38 HCCs in the PC

No. of feeders	No. of tumors	Site	Origin	Tumor
1	29 (76.3%)	R	R_1	4
			R_2	7
			A	3
			P	6
		L	L_1	1
			L_2	5
			M	3
2	7 (18.4%)	R + L	A, L_1	1
			P, L_1	1
			P, L_2	1
		R × 2	R_2, P	1
			A × 2	1
			A, P	2
3	2 (5.3%)	R × 3	R_1, A, P	1
			R_2, A, P	1

Mean tumor diameter 20.2 ± 9.3 mm [range 8–47]. The ratio of R:L = 37:12

segmental artery of the right hepatic artery and the left hepatic artery in 32.1% of 106 cadavers; from the posterior segmental artery of the right hepatic artery and the middle hepatic artery in 26.4% of cadavers; and from these three arteries in 20.8% of cadavers. In another cadaver study by Suzuki [11], the right-side caudate artery arose from the posterior segmental artery of the right hepatic artery in 89.7% of cadavers, and only 9.3% arose from the right hepatic artery. However, in previous angiographic observations, the most common origin of the caudate artery was the right hepatic artery [7–9]. In addition, the incidences of the caudate artery derived from the left hepatic artery and the posterior segmental artery of the right hepatic artery were low compared with those reported in dissection studies [7]. The cause of this discrepancy between dissection study and angiographic study is speculated as follows: First, the caudate artery derived from the right hepatic artery can easily be identified on arteriogram because there is less superimposition of the hepatic branches. Second, because the left hepatic lobe has a limited depth, identification of the caudate artery is difficult even on stereo angiogram [7]. Finally, the caudate artery derived from the posterior segmental artery is frequently difficult to recognize as the caudate artery on arteriogram because it mimics the branches of the posterior segmental artery of the right hepatic artery [7]. Therefore, there is a significant limitation in nonselective angiographic evaluations of the caudate arteries. Moreover, some small caudate branches derived from the proximal portion of the hepatic artery might be killed during preparation in dissection studies.

With advances in catheter technology, superselective catheterization and chemoembolization at the most distal level of the subsegmental artery of the liver have become possible [14, 15], even through the caudate arteries [9, 12, 16]. Iodized oil injected during the TACE procedure can clearly indicate the vascular territory of the embolized branch on CT. In the present study, we could easily recognize that the embolized branch was the caudate artery when iodized oil was retained in the caudate lobe, including the tumor, on CT obtained 1 week after TACE. This evaluation method facilitates precise identification of the caudate artery, although this artery frequently mimics other hepatic branches on arteriogram alone.

In the present study, the most frequent origin of the tumor-feeding caudate artery was the right hepatic artery, followed with almost equal frequency by the left hepatic artery, the anterior segmental artery, and the posterior segmental artery of the right hepatic artery. Our results suggest that the caudate artery actually can be identified from the right hepatic artery most frequently and not just because it can easily be identified on arteriogram due to less superimposition of the hepatic branches. Among the caudate arteries derived from the right and left hepatic arteries, it dominantly arose from the distal portion (R_2 and L_2). In addition, the ratio of the caudate artery origin of the right hepatic arterial system to the left hepatic arterial system was 2.6:1. However, HCCs in the CP were fewer than those in the SP and the PC in the present study. If our cohort had included more tumors in the CP, the number of caudate arteries derived from the right hepatic arterial system might have increased.

The origins of the tumor-feeding caudate arteries may differ among the three subsegment locations of HCC [8, 9, 12]. In the present study, HCCs located in the SP were fed from the caudate arteries derived from the right and left hepatic arterial systems (the ratio of right to left = 3:2). In addition, the extrahepatic vessels infrequently feed HCCs in the SP, in particular those located at the liver surface. HCCs in the PC were also fed by the caudate arteries derived from the right and left hepatic arterial systems, with a lower frequency arising from the left hepatic arterial supply (the ratio of right to left = 3:1). Almost all HCCs in the CP were dominantly fed by the caudate artery derived from the right hepatic arterial system, mainly arising from the anterior or posterior segmental artery of the right hepatic artery. This tendency may be helpful to identify the tumor-feeding caudate artery according to the tumor location. Yoon et al. [9] also reported a similar tendency, although the incidences of blood supply to HCCs in the PC from the left hepatic arterial system were low compared with those in our series. We selected patients with HCCs in the caudate lobe that had not previously been treated. However, 62% of patients had previously undergone TACE for other HCCs before detection of HCCs in the

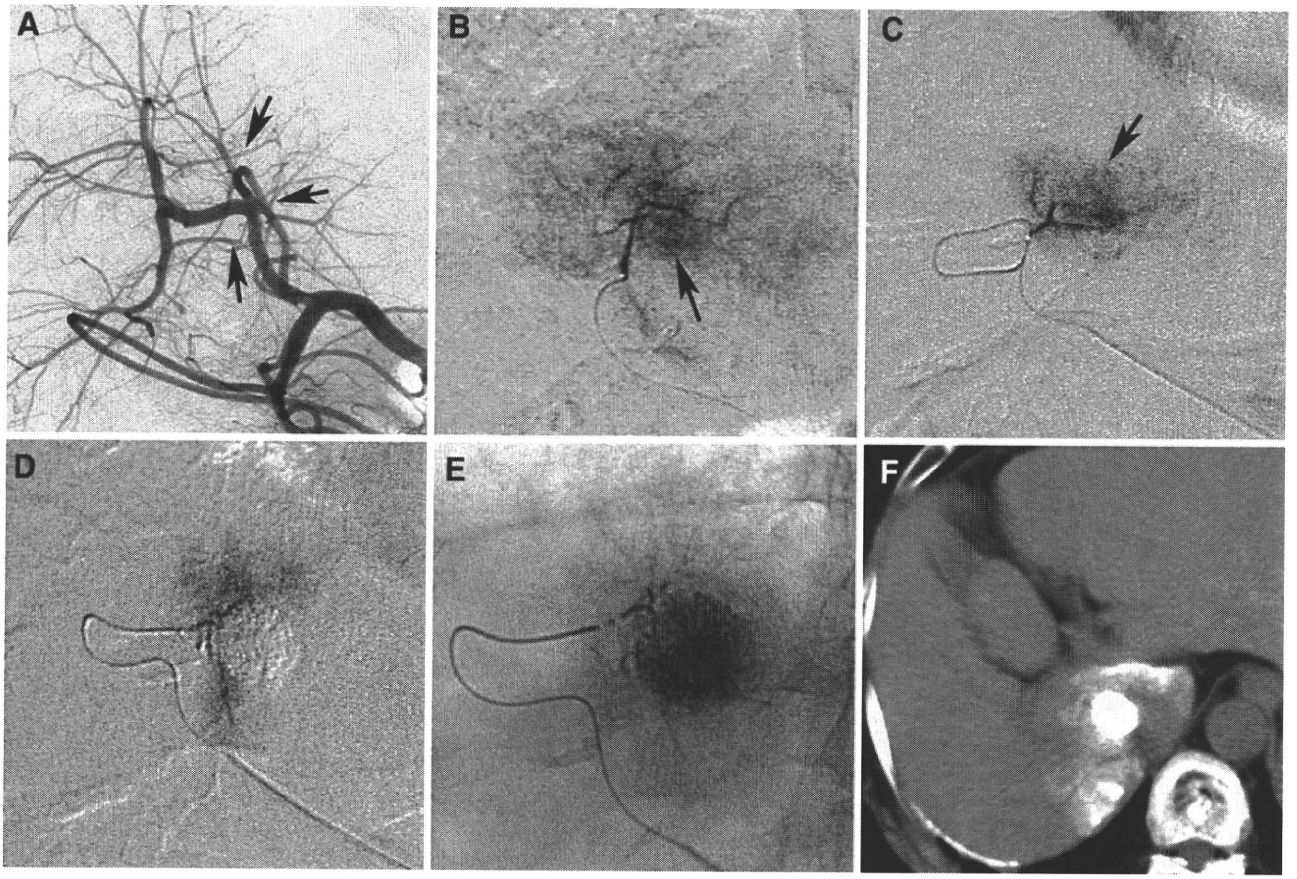

Fig. 6 A 75-year-old woman with HCC in the PC. **A** Celiac arteriogram showed three caudate arteries (*arrows*). **B** The caudate artery derived from the distal portion of the right hepatic artery was selected and arteriogram showed a tumor stain (*arrow*). TACE was performed at this point. **C** The caudate artery deriving from the posterior segmental artery of the right hepatic artery was selected, and the arteriogram also showed a tumor stain (*arrow*). TACE was performed. **D** The caudate artery deriving from the anterior segmental artery of the right hepatic artery was selected, and TACE was performed. **E** Spot radiograph obtained during TACE showed dense iodized oil accumulation in the tumor. **F** CT obtained 1 week after TACE showed dense iodized oil accumulation in HCC and the caudate lobe

Table 4 Feeding arteries of 14 HCCs in the CP

No. of feeders	No. of tumors (%)	Site	Origin	Tumor
1	9 (64.3)	R	R_1	1
			A	3
			P	3
		M	M	1
		Ph	Ph	1
2	4 (28.6)	R × 2	R_1, R_2	1
			R_2, A	1
			A × 2	1
			P × 2	1
3	1 (7.1)	R × 3	R_2, P × 2	1

Mean tumor diameter 21.8 ± 12.9 mm [range 12–49]

caudate lobe. Previous TACE through the neighboring branches of the caudate lobe might have changed the vascular territories of the caudate arteries.

There are several limitations in the present study. First, we did not evaluate the caudate arteries that were identified on arteriogram, but that did not supply the tumor, because we could not definitely confirm whether these vessels exactly supplied the caudate lobe on angiographic findings alone. Therefore, our study did not analyze the origins of all of the caudate arteries, and this might strongly influence the number and origin of the caudate arteries detected. Three-dimensional CT during hepatic arteriography, using a multidetector-row CT, may provide sufficient information about the caudate arteries, including those that do not supply the tumor. Second, the number of tumor-feeding caudate arteries might easily change according to the tumor size. In large tumors, small caudate branches may become hypertrophied enough to be depicted on arteriogram, and parasitization of the extrahepatic collateral vessels may also become apparent. Finally, there was a possibility of missing small tumor-feeding caudate branches, although iodized oil was accumulated in all tumors throughout the

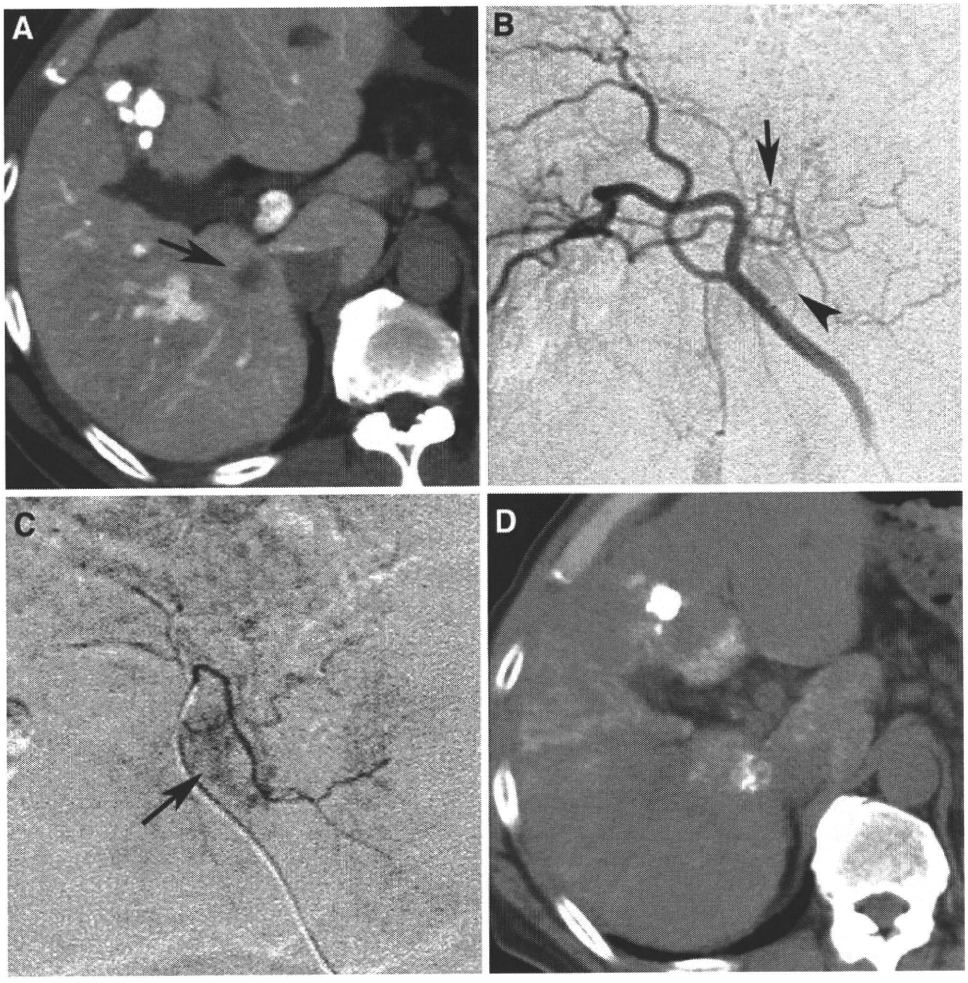

Fig. 7 A 64 year-old man with HCC in the CP. **A** CT during arterial portography showed a tumor in the CP (*arrow*). The tumor with iodized oil accumulation that had previously been embolized was also seen in segment 4. **B** Arteriogram of the right hepatic artery showed that the caudate artery derived from the posterior segmental artery of the right hepatic artery (*arrow*). The *arrowhead* shows a tumor stain. **C** The caudate artery was selected and embolized. The *arrow* showed a tumor stain. **D** CT obtained 1 week after TACE showed iodized oil accumulation in HCC in the CP

entire tumor portion after TACE, including those after six additional TACE sessions. Because multiple caudate arteries are frequently connected not only with each other but also with neighboring branches, iodized oil might also flow into the tumor through unidentified small caudate branches by way of these communications [16, 17].

In conclusion, the tumor-feeding caudate artery most frequently arose from the right hepatic artery, followed with almost equal frequency by the left hepatic artery, the anterior segmental artery of the right hepatic artery, and the posterior segmental artery of the right hepatic artery. HCCs located in the SP were fed by the caudate artery derived from both hepatic arteries (the ratio of right to left = 3:2); HCCs in the PC were also fed by both hepatic arteries (the ratio of right to left = 3:1); and HCCs in the CP were dominantly fed by the caudate artery derived from the right hepatic artery. We consider that recognition of this tendency may be helpful to identify the tumor-feeding caudate artery on angiogram.

Conflict of Interest None.

References

1. Takayasu K, Muramatsu Y, Shima Y et al (1986) Clinical and radiologic features of hepatocellular carcinoma originating in the caudate lobe. Cancer 58:1557–1562
2. Tanaka S, Shimada M, Shirabe K et al (2005) Surgical outcome of patients with hepatocellular carcinoma originating in the caudate lobe. Am J Surg 190:451–455
3. Shimada M, Matsumata T, Maeda T et al (1994) Characteristics of hepatocellular carcinoma originating in the caudate lobe. Hepatology 19:911–915

4. Shibata T, Maetani Y, Ametani F et al (2002) Efficacy of non-surgical treatments for hepatocellular carcinoma in the caudate lobe. Cardiovasc Intervent Radiol 25:186–192
5. Seror O, Haddar D, N'Kontchou G et al (2005) Radiofrequency ablation for the treatment of liver tumors in the caudate lobe. J Vasc Interv Radiol 16:981–990
6. Yamakado K, Nakatsuka A, Akeboshi M et al (2005) Percutaneous radiofrequency ablation for the treatment of liver neoplasms in the caudate lobe left of the vena cava: electrode placement through the left lobe of the liver under CT-fluoroscopic guidance. Cardiovasc Intervent Radiol 28:638–640
7. Miyayama S, Matsui O, Kameyama T et al (1990) Angiographic anatomy of arterial branches to the caudate lobe of the liver: with special reference to its effect on transarterial embolization of hepatocellular carcinoma. Jpn J Clin Radiol 35:353–359 (in Japanese)
8. Terayama N, Miyayama S, Tatsu H et al (1998) Subsegmental transcatheter arterial embolization for hepatocellular carcinoma in the caudate lobe. J Vasc Interv Radiol 9:501–508
9. Yoon CJ, Chung JW, Cho BH et al (2008) Hepatocellular carcinoma in the caudate lobe of the liver: angiographic analysis of tumor-feeding arteries according to subsegmental location. J Vasc Intev Radiol 19:1543–1550
10. Mizumoto R, Suzuki H (1988) Surgical anatomy of the hepatic hilum with special reference to the caudate lobe. World J Surg 12:2–10
11. Suzuki H (1982) Correlation and anomalies of the vascular stricture in Glisson's area around the hepatic hilum, from the standpoint of hepatobiliary surgery. Arch Jpn Chir 51:713–731 (in Japanese)
12. Miyayama S, Yamashiro M, Yoshie Y et al (2010) Hepatocellular carcinoma in the caudate lobe of the liver: variations of its feeding branches on arteriography. Jpn J Radiol 28:555–562
13. Kumon M (1985) Anatomy of the caudate lobe with special reference to portal vein and bile duct. Acta Hepatol Jpn 26:1193–1199 (in Japanese)
14. Matsui O, Kadoya M, Yoshikawa J et al (1993) Small hepatocellular carcinoma: treatment with subsegmental transcatheter arterial embolization. Radiology 188:79–83
15. Miyayama S, Matsui O, Yamashiro M et al (2007) Ultraselective transcatheter arterial chemoembolization with a 2-F tip microcatheter for small hepatocellular carcinomas: relationship between local tumor recurrence and visualization of the portal vein with iodized oil. J Vasc Interv Radiol 18:365–376
16. Miyayama S, Yamashiro M, Okuda M et al (2010) Main bile duct stricture occurring after transcatheter arterial chemoembolization for hepatocellular carcinoma. Cardiovasc Intervent Radiol 33: 1168–1179
17. Miyayama S, Matsui O, Taki K et al (2005) Arterial blood supply to the posterior aspect of segment IV of the liver from the caudate branch: demonstration at CT after iodized oil injection. Radiology 237:1110–1114

Cardiovasc Intervent Radiol (2011) 34:81–86
DOI 10.1007/s00270-010-9835-9

CLINICAL INVESTIGATION

Detection of Corona Enhancement of Hypervascular Hepatocellular Carcinoma by C-Arm Dual-Phase Cone-Beam CT During Hepatic Arteriography

Shiro Miyayama · Masashi Yamashiro · Miho Okuda · Yuichi Yoshie · Yoshiko Nakashima · Hiroshi Ikeno · Nobuaki Orito · Osamu Matsui

Received: 12 December 2009 / Accepted: 18 February 2010 / Published online: 24 March 2010
© Springer Science+Business Media, LLC and the Cardiovascular and Interventional Radiological Society of Europe (CIRSE) 2010

Abstract The purpose of this study was to evaluate the detectability of corona enhancement around the hypervascular hepatocellular carcinoma (HCC) by dual-phase cone-beam computed tomography during hepatic arteriography (CBCTHA). Dual-phase CBCTHA was performed for 71 HCC lesions (mean ± SD 1.7 ± 0.9 cm), including seven presenting a nodule-in-nodule appearance and nine hypervascular pseudolesions. The first scan was performed during injection of 30–40 ml half-diluted contrast material at a rate of 1.5–2 ml/s through the hepatic artery. Scanning was initiated 7 s after the beginning of contrast material injection. The second scan was started 30 s after the end of the first scan. Detectability of corona enhancement on second-phase CBCTHA was evaluated. Thickness of corona enhancement was also analyzed as thin (≤2 mm) or thick (>2 mm). Corona enhancement was detected in 63 (88.7%) of 71 tumors (1.8 ± 0.9 cm), but it was not detected in eight tumors (1.0 ± 0.2 cm). Thin corona enhancement was seen in 18 tumors (1.2 ± 0.5 cm), and thick corona enhancement was seen in 45 tumors (2.0 ± 0.9 cm). There was a significant difference in tumor diameter between tumors with and those without corona enhancement ($P = 0.0157$) and between thin and thick corona enhancement ($P = 0.001$). In all seven early-stage tumors, corona enhancement was demonstrated around the hypervascular focus within the hypovascular tumor portion. None of the nine pseudolesions showed any corona enhancement. Dual-phase CBCTHA depicted corona enhancement in 88.7% of hypervascular HCC lesions. This technique may improve the diagnostic accuracy of HCC.

Keywords Hepatocellular carcinoma · Corona enhancement · Cone-beam CT

S. Miyayama (✉) · M. Yamashiro · M. Okuda · Y. Yoshie · Y. Nakashima · H. Ikeno · N. Orito
Department of Diagnostic Radiology,
Fukuiken Saiseikai Hospital, Fukui 918-8503, Japan
e-mail: s-miyayama@fukui.saiseikai.or.jp

O. Matsui
Department of Radiology, Graduate School of Medical Science,
Kanazawa University, Kanazawa 920-8641, Japan

Introduction

Corona enhancement is one of the characteristic findings of hypervascular hepatocellular carcinoma (HCC) on late-phase computed tomography during hepatic arteriography (CTHA) and single-level dynamic CTHA [1–5]. On single-level dynamic CTHA, corona enhancement around the HCC lesion appears between 22 and 40 s after contrast material injection [1]. This finding is also helpful to distinguish between HCC and other hypervascular pseudolesions, such as arterioportal shunts, which do not require treatment [2].

C-arm cone-beam CT (CBCT) is an alternative technology for obtaining CT-like images using an angiographic unit equipped with a flat panel detector (FPD) [6–9]. We have applied this technique to assist transcathater arterial chemoembolization (TACE) for HCC. In our previous reports, CBCT during hepatic arteriography (CBCTHA) had sufficient image quality to detect almost all of the small HCC lesions [8, 9]. In our CBCT protocol (XperCT; Philips Medical Systems, Best, The Netherlands), the second CBCT scan could be performed 90 s after the end of the first scan, just as corona enhancement would be expected to disappear. Two separate scans and two contrast material injections may be necessary to depict both tumor

stain and corona enhancement; however, this may increase the procedural time and total amount of contrast material.

Recently, a prototype of dual-phase CBCT software has been made available by the manufacturer. In this report, the detectability of corona enhancement of HCC by dual-phase CBCTHA technique was analyzed.

Materials and Methods

Patients

Between August and October 2009, TACE for HCC was performed in 66 patients. Among these, we performed dual-phase CBCTHA in 30 patients with newly developed tumors <5 cm in diameter. Our Institutional Review Board approved the use of a prototype of the dual-phase CBCT software (Philips). Written informed consent was obtained from each patient before the procedure. There were 17 men and 13 women (mean patient age 72.1 ± 7.9 years [range 48–85]). All patients had chronic hepatitis or liver cirrhosis. This was related to hepatitis C in 21 patients and to hepatitis B in four patients. In one patient, cirrhosis was related to both hepatitis B and C. In another patient, it was related to alcoholism. The etiology was unknown in three patients. The diagnosis of HCC was established by CT and/or magnetic resonance imaging findings, i.e., characteristic nodular enhancement on the arterial-phase and wash out on delayed-phase images, in addition to nodular stain on angiography. All patients had 1–8 tumors (mean 2.4 ± 1.7). Seven tumors were early-stage HCC presenting hypervascular foci within a hypovascular tumor portion, a so called nodule-in-nodule appearance. In such tumors, the diameter of the hypervascular focus was defined as the tumor diameter. In total, 71 tumors with a mean diameter 1.7 ± 0.9 cm (range 0.8–4.6) were found. Nine hypervascular pseudolesions, such as arterioportal shunts that were defined as showing early enhancing lesions with an amorphous shape or wedge-shape on arterial-phase CT and isoattenuating on unenhanced and delayed-phase CT, were also seen in eight patients.

Technique of Dual-Phase CBCT

An angiographic unit with a 38 × 30 cm^2 FPD (Allula Xper FD20; Philips) was used to obtain dual-phase CBCT images. Three hundred twelve projection images with X-ray parameters of 120 kV and 50–325 mA were obtained by 10.4-s acquisition with 207° rotation of the FPD of the angiographic C-arm around the patient. The radiation dose of a single CBCT measured on a CT phantom was 22.3 mGy. The first-phase was scanned during a clockwise rotation, and the second-phase was scanned during a counterclockwise rotation. The minimum interval between the end of the first scan and the start of the second scan was 4 s.

Angiography Protocol

CT during arterial portography (CBCTAP) was routinely performed at the beginning of the procedure. Forty milliliters of contrast material (370 mg I/ml iopamidol [Iopamiron 370; Bayer, Osaka, Japan] or 350 mg I/ml iomeprol [Iomeron 350; Ezai, Tokyo, Japan]) was injected at a rate of 3 ml/s through a 4F catheter placed into the superior mesenteric artery after administration of 2.5 μg prostaglandin E1 (Liple; Mitsubishi Pharma Corporation, Osaka, Japan). When replaced hepatic branches or arterial flow toward the liver from the superior mesenteric artery was demonstrated, the catheter tip was deeply advanced to avoid these branches. Scanning began 25 s after the beginning of contrast material injection, and a single-phase scan was obtained.

Dual-phase CBCTHA was obtained after CBCTAP, superior mesenteric arteriography, celiac arteriography, and common or proper hepatic arteriography. The first-phase CBCTHA was scanned during injection of 30–40 ml half-diluted contrast material at a rate of 1.5–2 ml/s through a 4F catheter placed into the common or proper hepatic artery of the liver. Scanning was initiated 7 s after the start of contrast material injection. The second-phase CBCTHA was started 30 s after the end of the first scan.

Three millimeter-thick CT-like images were obtained for observation of CBCT images on a workstation (Philips). Oxygen was administered to patients during the procedure to minimize the discomfort of breath holding.

Data Analysis

Dual-phase CBCTHA images were compared and evaluated to determine whether corona enhancement was depicted around the hypervascular tumor on the second-phase CBCTHA. Thickness of corona enhancement was also divided into two categories: thin (≤2 mm) and thick (>2 mm). The workstation did not have a measuring function; therefore, the thickness was measured using another viewer (ShadeQuest; Yokogawa Electric Corporation, Tokyo, Japan) and compared with conventional CT images. The diameters of tumors with and without corona enhancement and of tumors with thin and thick corona enhancement were statistically compared using Student t test, and $P < 0.05$ were considered significant. In addition, whether or not corona enhancement was depicted around the hypervascular pseudolesions was also evaluated.

Results

All tumors were detected as hypoattenuating lesions on CBCTAP and as hyperattenuating lesions on first-phase CBCTHA. In seven tumors showing a nodule-in-nodule appearance, the hypervascular focus on dynamic CT study was seen as hypoattenuating on CBCTAP and as hyperattenuating on first-phase CBCTHA.

Corona enhancement was detected in 63 of 71 HCC lesions (88.7%), with a mean diameter of 1.8 ± 0.9 cm (range 0.8–4.6) on second-phase CBCTHA images (Figs. 1, 2 through 3). Thin corona enhancement was seen in 18 tumors (mean diameter 1.2 ± 0.5 cm [range 0.8–2.6]), and thick corona enhancement was seen in 45 tumors (mean diameter of 2.0 ± 0.9 cm [range 0.9–4.6]). There was a significant difference in tumor diameter between thicknesses of corona enhancement ($P = 0.001$). Eight tumors with a mean diameter of 1.0 ± 0.2 cm (range 0.8–1.3) did not show any corona enhancement. There was a significant difference in tumor diameter between tumors with or without corona enhancement ($P = 0.0157$). In all seven early-stage tumors with a hypovascular portion around the hypervascular portion, corona enhancement was demonstrated around the hypervascular portion within the hypovascular tumor portion (Fig. 3).

Six (66.7%) of nine hypervascular pseudolesions showed slight diffuse enhancement on second-phase CBCTHA images. The remaining three lesions showed isoattenuation (Fig. 1). Corona enhancement was not seen in any of these lesions.

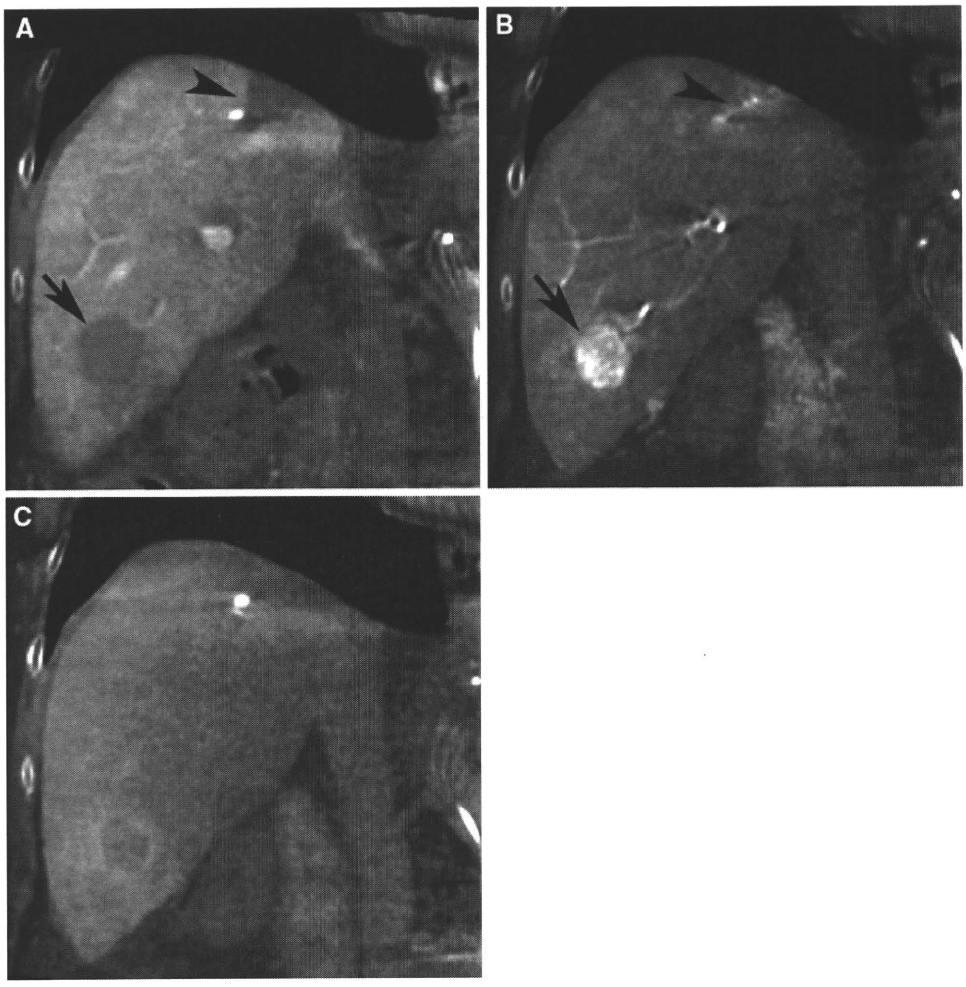

Fig. 1 HCC (2.2-cm diameter) and arterioportal shunt in the right lobe of the liver. **A** Coronal CBCTAP showed a nodular hypoattenuating lesion (HCC) (*arrow*) and wedge-shaped hypoattenuating lesion (*arrowhead*) adjacent to the tumor with iodized oil accumulation, which had previously been treated by TACE. **B** On coronal first-phase CBCTHA, HCC showed a nodular enhancement (*arrow*). The lesion near the iodized oil accumulated tumor showed wedge-shaped enhancement, including early appearance of the portal vein (*arrowhead*), suggesting an arterioportal shunt. **C** On coronal second-phase CBCTHA, thick corona enhancement was seen around the HCC nodule. The arterioportal shunt showed isoattenuation

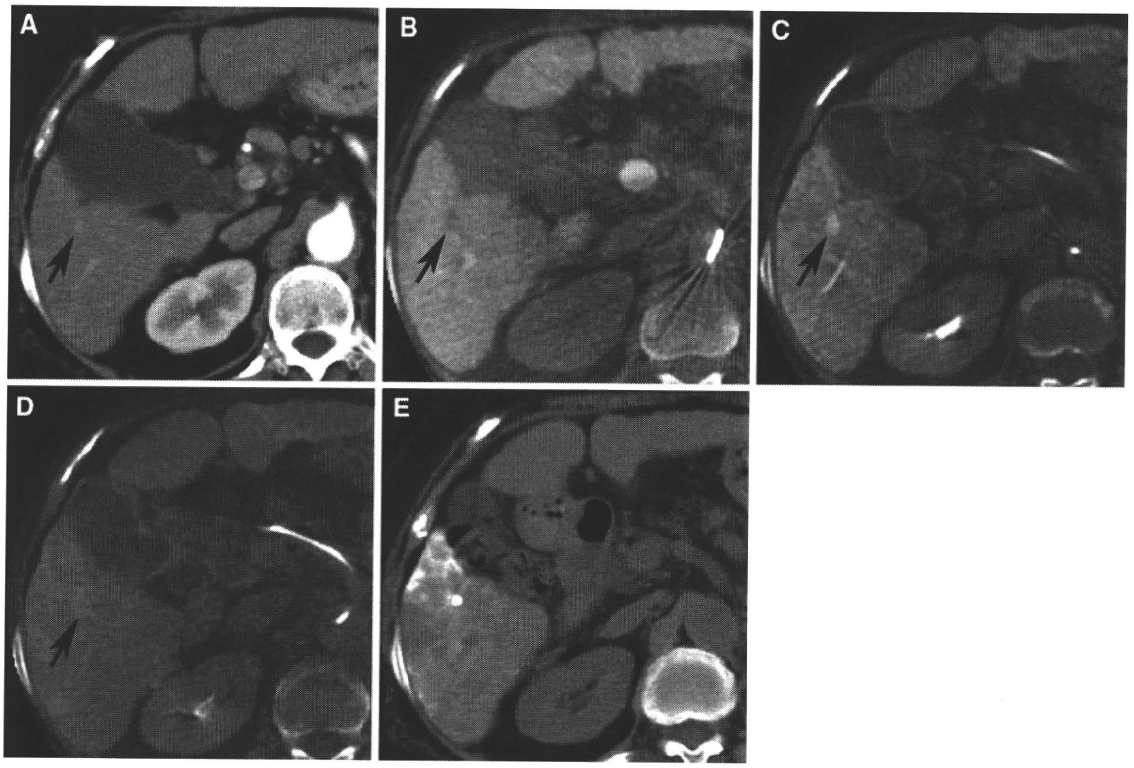

Fig. 2 Small HCC (8-mm diameter) in the right lobe of the liver. **A** Arterial-phase CT showed a small hyperattenuating lesion in the right lobe of the liver (*arrow*). **B** CBCTAP showed a nodular hypoattenuating lesion corresponding to the small lesion on CT (*arrow*). **C** On first-phase CBCTHA, the lesion showed nodular enhancement (*arrow*). **D** On second-phase CBCTHA, thin corona enhancement was seen around the lesion (*arrow*). The lesion was diagnosed as HCC and TACE was performed. **E** CT obtained 1 week after TACE showed dense iodized oil accumulation in the lesion

Discussion

Ueda et al. [1] named the wash of contrast material around hypervascular HCC lesions demonstrated on the late phase of single-level dynamic CTHA images as "corona enhancement." In a report by Kitao et al. [5], the drainage vessels of HCC change during multistep hepatocarcinogenesis. As the tumor cells become atypical and proliferate more rapidly, they first invade the intranodular hepatic veins and then compress the perinodular hepatic veins. As a result of hepatic vein occlusion, the tumor blood begins to drain into the hepatic sinusoids and portal veins. In hypervascular HCCs without a tumor capsule, direct drainage from tumor sinusoids to adjacent hepatic sinusoids is seen as thin corona enhancement (≤2 mm). In hypervascular HCCs with a tumor capsule, perinodular hepatic sinusoids have collapsed, and continuity of intranodular and extranodular sinusoids is interrupted by the capsule. Therefore, tumor blood drains into the surrounding liver parenchyma through the preserved portal veins within the capsule, and thick corona enhancement (>2 mm) is demonstrated. Corona enhancement is one of the characteristic findings of hypervascular HCCs, but it is also seen around metastatic liver tumors [3, 10]. In contrast, corona enhancement is not seen around hypervasucular pseudolesions, such as arterioportal shunts. Therefore, corona enhancement is one of the most reliable findings to distinguish between liver tumors and arterioportal shunts [2].

In the present study, corona enhancement was depicted in 88.7% of HCC lesions on second-phase CBCTHA images. The minimum-diameter corona enhancement demonstrated was 0.8 cm. Thick corona enhancement was seen in relatively large tumors and might represent the rich tumor vascularity and tumor capsule formation. In addition, in seven tumors showing a nodule-in-nodule appearance, corona enhancement was seen within the hypovascular tumor portion around the hypervascular focus. This finding suggests that tumor blood of the hypervascular focus drains into the tumor sinusoids of the hypovascular portion with preserved portal vasculatures, as reported by Kita et al. [11]. This finding may also explain iodized oil accumulation in the hypovascular tumor portion after ultraselective TACE, as we previously reported [12]. Arterioportal shunts showed slightly prolonged enhancement of the entire lesion in 67% of lesions and did not show corona enhancement in any lesion. These findings helped to differentiate arterioportal shunts from hypervascular HCC lesions.